# Nuclear relaxation and antiferromagnetic critical effects in organic conductors

C. Bourbonnais

*Laboratoire de Physique des Solides, Université de Paris—Sud, 91405 Orsay Cédex, France*
*and Centre de Recherches en Physique des Solides, Université de Sherbrooke, Sherbrooke, Québec, Canada J1K 2R1*

P. Stein, D. Jérome, and A. Moradpour

*Laboratoire de Physique des Solides, Université de Paris—Sud, 91405 Orsay Cédex, France*

We present and analyze $^1H$ relaxation data of the spin-density-wave transition on oriented ditetramethyltetraselenafulvalenium phosphorus hexafluoride [(TMTSF)$_2$PF$_6$] single crystals at ambient pressure. A detailed analysis of the methyl-group rotation contribution to the nuclear relaxation rate $T_1^{-1}$ is made in the temperature domain precursor to the transition. We show that the singular profile of $T_1^{-1}$ can be well described as an antiferromagnetic critical effect with a three-dimensional classical exponent. The scaling form of the critical quantity $(T_1T)^{-1}$ in low-dimensional antiferromagnets with a nesting vector exhibiting a dimensionality crossover in temperature is derived and discussed in connection with the data.

## I. INTRODUCTION

The spin-density-wave (SDW) state which exists at low temperature in some members of the ditetramethyltetraselenafulvalene [(TMTSF)$_2X$] family of organic conductors has been studied in some detail for the rather similar cases where $X = PF_6$ or $AsF_6$. This phenomenon is of functional interest, owing to it proximity to superconductivity in the general phase diagram of (TMTSF)$_2X$ compounds.

The possibility of a SDW low-temperature state at ambient pressure was first suggested by Walsh et al.,[1] on the basis of an observed nonlinearity of the electrical conductivity in the semiconducting ground state below $T_c \sim 12$ K. Although the meaning of these nonlinearities is still open to discussion,[2] magnetic effects have been detected in susceptibility and EPR measurements with only a small anomaly of the powder Faraday susceptibilities[3] but an abrupt vanishing of the EPR susceptibility at the transition.[4]

The SDW nature of the ground state has been firmly established by Faraday susceptibility studies of the anisotropies on (TMTSF)$_2$AsF$_6$ (Ref. 5) and (TMTSF)$_2$PF$_6$ (Ref. 6) single crystals. These measurements have also allowed the determination of the easy axis for the magnetization of the SDW state along the $b^*$ direction and a spin-flop field around 4.8 KOe at liquid-helium temperature. Additional spectroscopic studies of the magnetic modes have been provided by the observation of the electron antiferromagnetic resonance in the SDW state of (TMTSF)$_2$PF$_6$ (Ref. 7).

NMR techniques have also been used to study the SDW state. Direct evidence for a magnetic ground state comes from NMR experiments on $^{77}$Se ($I = \frac{1}{2}$) (Ref. 8). The NMR line in (TMTSF)$_2$PF$_6$ broadens inhomogeneously due to the occurrence of internal magnetic fields below 12 K and becomes too broad to be detected at lower temperatures.

Similarly, a broadening of the NMR line has been observed at 12 K for the $^1H$ of the methyl groups, but there, the nuclear resonance remains visible in the SDW state. The concomitant decrease of the $^1H$ homogeneous linewidth ($1/T_2$) demonstrates the inhomogeneous nature of the line broadening.

Among the few observable quantities that can give direct microscopic information about the singular nature of the electronic system both near and far from the SDW transition, the nuclear spin-lattice relaxation rate $T_1^{-1}$ is certainly one of the best probes for the characterization of magnetic correlations of all scales. As mentioned above, the proton resonance is the only resonance in (TMTSF)$_2$PF$_6$ which can be followed through the magnetic transition. NMR data have revealed an anomaly in $1/T_1(^1H)$ at the transition.[8,9] But since these results were obtained on powder samples, anisotropy effects and a proper determination of the critical profile of $1/T_1$ were altered in these experiments. Single-crystal work therefore appears to be necessary for the NMR study of anisotropic systems such as (TMTSF)$_2X$. Thus, we present, in this work, the first $^1H$ relaxation-rate measurements on oriented (TMTSF)$_2$PF$_6$ performed through the SDW transition.

However, when studying proton resonance in (TMTSF)$_2X$ systems, great care should be taken concerning the origin of the mechanism for spin-lattice relaxation. Protons in these compounds all belong to methyl groups (CH$_3$) which can rotate around an axis. This methyl-group rotation is classically thermally activated at high temperature and can be described by quantum tunneling at low temperature.[9] The resulting time-dependent modulation of the H-H dipolar interaction within each CH$_3$ group therefore becomes a powerful channel for $^1H$ spin-lattice relaxation which can, under certain circumstances, mask the effects in which we are particularly interested in the present study, namely, the influence of electron-spin correlations on the $^1H$ spin-lattice relaxation.

The relaxation due to methyl rotation becomes negligible at high temperature when the $CH_3$ motion becomes fast compared to the nuclear Larmor frequency.[9] A damping of the rotation- (or quantum-tunneling-) induced relaxation is also expected at low temperatures. However, a careful study of the temperature dependence of $1/T({}^1H)$ must be performed below 30 K in order to evaluate the relative weight of extrinsic ($CH_3$ rotation) and intrinsic relaxation mechanisms in the magnetic transition-temperature domain. The experimental section is devoted to the study of the ${}^1H$ relaxation below 30 K leading to the estimate of extrinsic relaxation in the low-temperature regime.

The behavior of $T_1^{-1}$ around the SDW transition is then analyzed in terms of a power-law divergence at $T_c$. The theory section presents a model which strongly supports that $1/T_1$ near $T_c$ is dominated by SDW critical fluctuations and, accordingly, that quasiparticles do not contribute significantly to the relaxation in this region.[10] For the model considered, scaling properties are found to be compatible with a general prediction of the theory of critical phenomena for anisotropic systems. The results obtained should apply to all SDW phases of the $(TMTSF)_2X$ series with nesting properties which undergo a dimensionality crossover.

## II. EXPERIMENTAL RESULTS

The measurements were performed with a single crystal of typical size $5 \times 0.5 \times 0.5$ mm$^3$, with respect to temperature at various magnetic field magnitudes and orientations in the plane perpendicular to the $a$ axis of the single crystal. The magnetic field values, namely, 2.6, 4.1, 5.2, and 6.4 kOe, were chosen to be above and below the spin-flop field of 4.8 kOe.[6] For these field values, the relaxation rate was measured with a $\pi$-$\pi/2$ pulse sequence or a spin-echo technique. The recovery of the magnetization followed an exponential time dependence in terms of the change of the dependent variable. The relative stability of the temperature between different measurements was better than 0.2 K. Figure 1 gives the relaxation rate versus temperature between 30 and 10 K at different magnetic fields. The frequency-dependent peak of $1/T_1$ in the vicinity of 20 K can be attributed to the $CH_3$ rotation and the anomaly near 11 K is related to the SDW transition. Above 50 K, $1/T_1$ shows qualitatively the same temperature dependence observed for $(TMTSF)_2ClO_4$ (Ref. 9) with a peak and a shoulder at 55 and 75 K, respectively.

The theory of relaxation via $CH_3$ rotation has been largely developed by Clough[11] with the following result for $1/T_1$:

$$\frac{1}{T_1} = C_1 \left[ \frac{\tau}{1+\omega_n^2\tau^2} + \frac{4\tau}{1+4\omega_n^2\tau^2} \right]$$
$$+ C_2 \left[ \frac{\tau}{1+(1-\alpha)^2\omega_n^2\tau^2} \right] + \frac{4\tau}{1+(2-\alpha)^2\omega_n^2\tau^2}$$
$$+ \frac{\tau}{1+(1+\alpha)^2\omega_n^2\tau^2} + \frac{4\tau}{1+(2+\alpha)^2\omega_n^2\tau^2} , \quad (1)$$


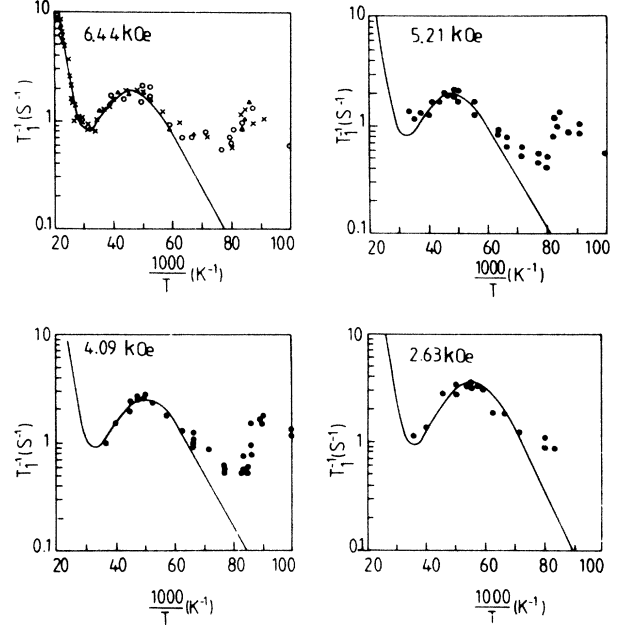
FIG. 1. Relaxation rate $(T_1^{-1})$ of $(TMTSF)_2PF_6$ versus the temperature for magnetic fields 2.63 kOe (11.2 MHz), 4.09 kOe (17.4 MHz), 5.21 kOe (22.2 MHz), and 6.44 kOe (27.4 MHz). The results at 6.44 kOe are given for different orientations of the field in the $b' \times c^*$ plane: $\times$, 90° $(c^*)$; $\triangle$, 60°; $\blacktriangle$, 45°, $\square$, 30°; $\bullet$ and $\bigcirc$, 0° $(b')$. The curves are plotted with the aid of Eq. (1) and values of Table I.

where $\omega_n$ is the nuclear Larmor frequency, $\alpha = \omega_t/\omega_n$, $\omega_t$ is the tunneling frequency, and $\tau$ is the thermally activated reorientation time, $\tau = \tau_0\exp(E/T)$, with $E$ the activation energy.

In Eq. (1), the $C_1$ and $C_2$ terms describe the classical reorientation contribution in the three-modal potential and the quantum-tunneling contribution, respectively. Figures 2(a) and 2(b) show the frequency dependence of the $1/T_{1\,max}$ peak value and of the temperature $T_0$ where this peak arises.

First, we can eliminate quantum tunneling with $\omega_t \gg \omega_n$ as the dominant source of relaxation near 20 K, since if this were the case, $1/T_{1\,max}$ would be frequency independent in contradiction to the data in Fig. 2(a). Thus we are left for the interpretation of $1/T_1$ in the vicinity of 20 K with two other possibilities:

(i) the relaxation is dominated by the classical term $C_1$ in Eq. (1);

(ii) quantum tunneling with $\omega_t \ll \omega_n$ is dominant.

In both cases, the activation energy $E$ can be derived from the frequency dependence of $T_0$ since

$$\frac{1}{T_0} \approx \frac{1}{E} \left[ \ln \left[ \frac{0.61}{\tau_0} \right] - \ln\omega \right] . \quad (2)$$

Data in Fig. 2(b) lead to $E = 120$ K. According to the theory of Clough,[11] 120 K is a small activation energy, providing $\omega_t \gg \omega_n$, in contradiction to the starting hypothesis (ii). Furthermore, recent ${}^1H$ line-shape data in $(TMTSF)_2X$ (Ref. 12) give no indication of fast quantum tunneling at low temperature. The relaxation rate in the
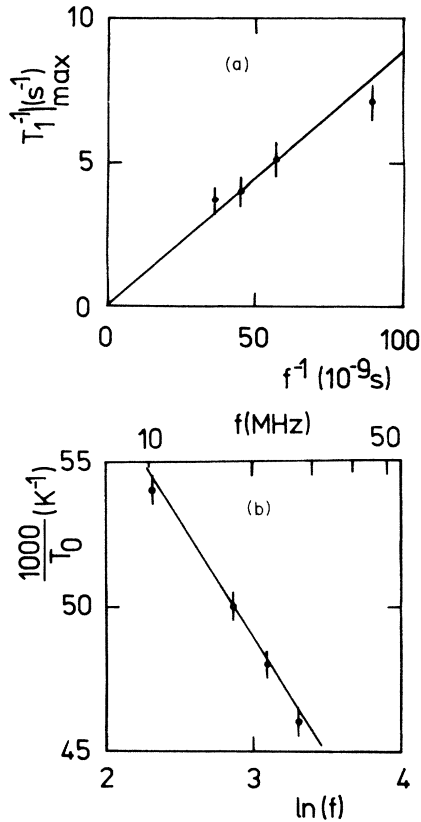
FIG. 2. (a) Frequency dependence of the maximum value for $T_1^{-1}(T_{1\,\mathrm{max}}^{-1})$ for the methyl-group contribution. (b) Frequency dependence for the temperature ($T_0$) for the occurrence of $T_{1\,\mathrm{max}}^{-1}$.

TABLE I. Values of $T_0(K)$ used for the analysis of the methyl-group contribution to the relaxation rate $T_1^{-1}$ at low temperature.

| $T_0$ (K) | $f$ (MHz) |
|-----------|-----------|
| 21.7 | 27.4 |
| 20.8 | 22.2 |
| 20.0 | 17.4 |
| 18.5 | 11.2 |

dence of $T_c$ has been reported on (TMTSF)$_2$AsF$_6$ single crystals.[5] The value of $T_1^{-1}$ at 13 K is about 0.5 s$^{-1}$ and field independent, in agreement with earlier powder data obtained at higher field (12 kOe),[8] where the CH$_3$ contribution is shifted towards higher temperatures ($\approx 25$ K).

Finally, we proceed to an analysis of the $1/T_1$ temperature dependence at the field of 6.44 kOe in the vicinity of $T_c$, Fig. 4. The log-log plot of $T_1^{-1}$ versus $(T-T_c)/T_c$ in the domain $T_c < T \le 13$ K gives the slopes $-0.4$, $-0.4$, and $-0.65$, corresponding, respectively, to the three field orientations in the $b'$-$c^*$ plane: 90° ($c^*$), 0° ($b'$), and 45°. Therefore, on average, $T_1^{-1}$ behaves like

$$T_1^{-1} \sim (\mid T - T_c \mid /T_c)^{-1/2} \quad (T_c = 11.3 \text{ K}) . \tag{3}$$

The data in the $T < T_c$ region are also aligned on a parallel line of slope $-\frac{1}{2}$ or so. With an error bar of approximately 10% for the $T_1^{-1}$ data, the critical form (3) thus reasonably describes *both* sides of the transition.

The $-\frac{1}{2}$ power-law divergence of $T_1^{-1}$ displayed on Fig. 4 at 6.44 kOe, is also true for other values of $H_0$.

20-K temperature region is thus determined by the classical contribution $C_1$ in Eq. (1), with the following set of parameters, $T_0 = 22$ K, $E = 120$ K, and $C_1 = 0.22 \times 10^9$ s$^{-2}$. Next, we have drawn, in Fig. 1, the theoretical contribution to the relaxation, which is expected from the classical reorientation at different magnetic fields, using data in Fig. 2 and the parameters of Table I. Hence, we feel confident in ascribing the sharp $T_1^{-1}(^1\mathrm{H})$ anomaly observed near 11 K to the onset of the SDW state with a negligible contribution coming from CH$_3$-group rotation.

In Fig. 3 we report $1/T_1$ data in the low-temperature regime (3.5—20 K) at different magnetic fields. We have also plotted the contribution to the relaxation coming from the CH$_3$ reorientation after the above-mentioned analysis. At all magnetic fields but 2.6 kOe, the temperature dependence of $1/T_1$ in the vicinity of $T_c$ is not influenced by extrinsic contributions. A slight anisotropy of $1/T_1$, for $H_0$ lying in the $b$-$c^*$ plane, is noticed at $T < T_c$ when $H_0$ is larger than the spin-flop field of 4.8 kOe.

When $H_0$ is smaller than the spin-flop field, the free induction decay (FID) can only be observed for $H_0 || c^*$. For other field orientations, the FID becomes too narrow to be detected ($T_2^* \approx 3$ μs) with our experimental setup. We have also noticed a small increase of $T_c$ when $H_0$ is varied through the spin-flop field ($T_c = 10.6$ and 11.3 K for $H_0 <$ or $> H_{\mathrm{SF}}$, respectively). A similar field depen-
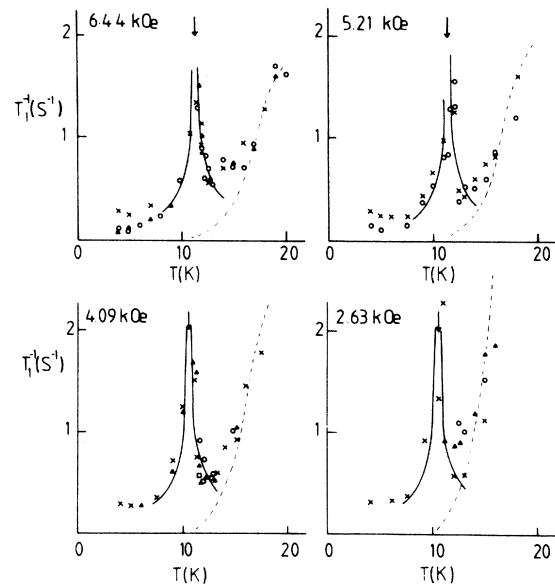


FIG. 3. Temperature dependence of the relaxation rate $T_1^{-1}$ in the vicinity of the antiferromagnetic transition for four values of the external field (see Fig. 1). The dashed lines represent the methyl-group contribution from the analysis of Fig. 1 and the solid guide lines are the electronic (critical) contribution to $T_1^{-1}$ in $(T - T_c)^{-1/2}$. For the field orientation, see Fig. 1.
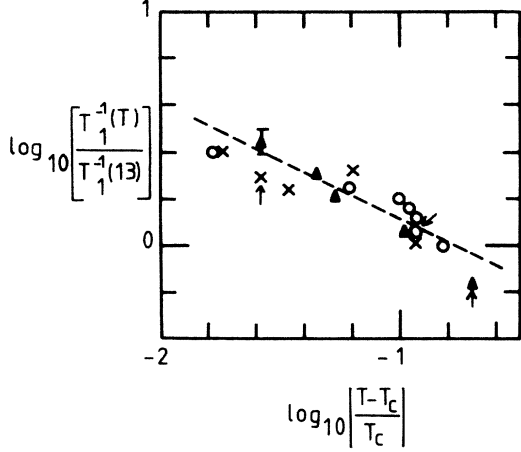
FIG. 4. Log-log plot of the relaxation rate $T_1^{-1}$ at 6.44 kOe normalized by the value taken at 13 K versus the critical temperature width $(T-T_c)/T_c$ with $T_c=11.3$ K. The dashed lines refer to the classical exponent $\frac{1}{2}$ for a three-dimensional antiferromagnet. Arrows refer to the data obtained at $T<T_c$. For the field orientation, see Fig. 1.

These results on $(TMTSF)_2PF_6$ single crystal contrast with the powder data,[8,9] which do not reveal a clear divergence at $T_c$, but rather show a somewhat asymmetric bump at the transition. This tends to prove that the direction of the field is probably relevant for the relaxation in the vicinity as well as below the transition. Although small, such an anisotropy is already present in the $b'$-$c^*$ plane at 6.4 kOe (cf. Fig. 3), but is expected to be bigger in the $a$ direction.

## III. THEORY

In order to specify the ingredients of our model for the evaluation of $T_1^{-1}$, which we want to be valid for all SDW transitions in $(TMTSF)_2X$ with two-dimensional (2D) or three-dimensional (3D) nesting, we must emphasize that the paramagnetic phase in these compounds is metallic and does not show any apparent resistivity minimum in contrast with antiferromagnets of the $(TMTTF)_2X$ series (where TMTTF denotes tetramethyl-tetrathiafulvalene).[13] This means that there is no gap for the charge degrees of freedom[14] and therefore a weak-coupling picture for the nesting properties of the quasi-1D electron gas is valid. For perfect nesting conditions, it predicts a SDW instability at finite temperature whenever the forward scattering part of the Coulomb interaction is repulsive $(g_2>0)$. In the present model (see also the end of Sec. IV), we will assume that the appearance of the 2D or 3D nesting properties coincides with the 1D to 2D dimensionality crossover temperature,[15]

$$T_x = T_x^0 (t_b/E_F)^{\Theta/(1-\Theta)} ,$$

where $T_x^0 = t_b/\pi$ is the free-electron-gas crossover temperature[16] with $t_b$ as the biggest transverse overlap integral oriented in the $b$ direction. Here we have assumed, for the electronic spectrum, a square lattice of weakly coupled tight-binding chains with $d_\perp$ as the transverse lat-
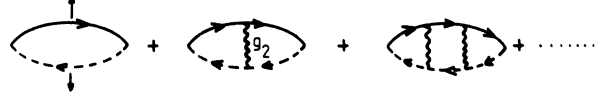


FIG. 5. Diagrammatic series for the SDW susceptibility $\chi$ in the random-phase approximation. The solid (dashed) lines refer to $+k_F$- $(-k_F-)$ going electrons. The arrows outside the elementary bubble $(\chi_0)$ are for the spin orientations. The wiggly line is the forward electron-electron scattering at $T_x[g_2(T_x)]$. For the 1D corrections to $\chi$, see the Appendix.

tice constant. $\Theta$ is an exponent that depends on Coulomb interactions.[15,17] In order to take into account the 1D fluctuation effects when $T>T_x$, it is preferable to use the effective value of $g_2$ given by the 1D renormalization-group equations at $T_x$.[17] In the present model, the effect of backward $(g_1)$ and umklapp $(g_3)$ scatterings are incorporated through additional renormalization of $g_2$ (Ref. 14) at $T_x$. In the following, the total effective coupling relevant to SDW at $T_x$ will be simply written as $g_2(T_x)$.

The general expression for $T_1^{-1}$ is given by[18]

$$T_1^{-1} = 2\gamma_N^2 T \sum_q A_q A_{-q} \chi_1''(q,\omega_N)/\omega_N , \qquad (4)$$

where $A_q$ is the hyperfine contact matrix element between the conduction electrons and the nuclear spins with $q$ as the transferred wave vector. $\omega_N = \gamma_N H_0$ is the nuclear Larmor frequency, $\gamma_N$ is the gyromagnetic ratio of the nucleus, and $H_0$ is the applied magnetic field. $\chi_1''$ is the imaginary part of the transverse susceptibility. Neglecting the magnetic anisotropy in $g_2(T_x)$, the quantity of interest becomes $\chi'''(q,\omega_N)/\omega_N$ in the limit $\omega_N \to 0$. As shown in the Appendix, within the random-phase approximation (RPA), the total imaginary part of the susceptibility of the system takes the form

$$\chi'(q,\omega_N) = \frac{Z_{1D}(T_x)\chi_0''(q,\omega_N)}{\{1+[g_2(T_x)/2]\chi_0'(q,\omega_N)\}^2} . \qquad (5)$$

Here, $\chi_0'(')$ is the bare real (imaginary) part of the susceptibility for wave vector $q$ near the perfect nesting vector $Q_0=(2k_F, \pi/d_\perp, \pi/d_\perp)$ of the SDW instability. The form (5) in the numerator coincides with the 1D $2k_F$ contribution to $\chi''$ in the limit $T \to T_x$ and $Z_{1D}(T_x)$ is a scaling factor that corresponds to the 1D $2k_F$ auxiliary susceptibility[19] at $T_x$ which is defined as

$$Z_{1D}(T) \equiv \pi V_F \frac{\partial \chi_{1D}'}{\partial \ln(T/E_0)} ,$$

where $E_F > E_0 > T$ is a cutoff energy. If we neglect the 1D corrections to $\chi$, $Z_{1D}=1$ and we recover from (A6) and (5), the usual RPA for $\chi$ as shown diagrammatically in Fig. 5.

If we insert the full expansion (5) into (4) we find

$$T_1^{-1} = 2\gamma_N^2 T Z_{1D}(T_x) \sum_q \frac{A_q A_{-q} \chi_0''(q,\omega_N)}{\omega_N\{1+[g_2(T_x)/2]\chi_0'(q,\omega_N)\}^2} , \qquad (6)$$

where the imaginary $(\chi_0'')$ and real $(\chi_0')$ parts of the element bubble in Fig. 1 are written, respectively, as

$$| A_{\mathbf{q}} |^2 \chi_0''(\mathbf{q}, \omega_N) = \frac{2\pi}{V} \sum_{\mathbf{k}} | A_{\mathbf{q}} |^2 \{ n[E_+(\mathbf{K})] - n[E_-(\mathbf{K}-\mathbf{q})] \} \delta(\omega_N - E_+(\mathbf{K}) + E_-(\mathbf{K}-\mathbf{q}))$$

$$= \pi \rho(E_F) \langle | A_{\mathbf{q}} |^2 \rangle_{\mathrm{FS}} \delta(\omega_N - E_+(\mathbf{K}_F) - E_-(\mathbf{K}_F - \mathbf{q})) , \qquad (7a)$$

where $n(x) = (e^{x/T} + 1)^{-1}$ and

$$\chi_0'(\mathbf{q}, \omega_N) = \frac{2}{V} \mathbf{P} \sum_{\mathbf{k}} \frac{n[E_+(\mathbf{K})] - n[E_-(\mathbf{K}-\mathbf{q})]}{E_+(\mathbf{K}) - E_-(\mathbf{K}-\mathbf{q}) - \omega_N} \simeq (\pi V_F)^{-1} \left[ \ln \left[ \frac{T}{E_0^{3D}} \right] + \xi_{0,a}^2(T) q_a^2 + \xi_{0,b}^2(T) q_b^2 + \xi_{0,c}^2(T) q_c^2 \right] . \qquad (7b)$$

$E_\pm(\mathbf{k})$ is the electronic energy for right- $(+)$ and left- $(-)$ going electrons near the open Fermi surface. $\rho(E_F)$ is the density of states at the Fermi level and $\langle | \overline{A}_q | \rangle_{\mathrm{FS}}$ stands for the average over the entire Fermi surface for the volume-independent hyperfine matrix element $\overline{A}_q = A_q / \sqrt{V}$. For $\chi_0$, we have taken a small-q expansion around $\mathbf{Q}_0$, since only long-wavelength SDW fluctuation modes give the dominant contribution to $\chi$ and $T_1^{-1}$ near the critical temperature $T_c = E_0^{3D} \exp[-2\pi V_F / g_2(T_x)]$, which is determined by the divergence of $\chi$ with (7b). If

the 3D nesting properties take place below $T_x$, one has $E_0^{3D} \sim T_x$. The characteristic length $\xi_{0,c}(T) \simeq 0.46 t_i d_i / T$ gives the shortest length considered for SDW fluctuation modes in the $i$ direction ($i = a$, $b$, and $c$). As far as the quasi-1D electronic spectrum of $(\mathrm{TMTSF})_2\mathrm{PF}_6$ is concerned, it is characterized by the anisotropic sequence $t_a \approx 3000 \mathrm{K} \approx 15 t_b \approx 450 t_c$.[20,21]

Around $T_c$, the sum over q in (6), with the constraint given in (7a), is made up to $\xi_i^{-1}(T_c)$ in the $i$ direction with the following result in three dimensions:

$$T_1^{-1} = \pi \gamma_N^2 T [\rho(E_F)]^2 \langle | \overline{A} |^2 \rangle_{\mathrm{FS}} Z_{1D}(T_x) \left[ \frac{d_a d_1^2}{\pi} [\xi_{0,a}(T_c) \xi_{0,b}(T_c) \xi_{0,c}(T_c)]^{-1} \right] r^{-1/2} , \qquad (8)$$

with

$$r = \frac{g_2(T_x)}{2\pi v_F} \ln(T/T_c) \cong \frac{g_2(T_x)}{2\pi v_F} \left[ \frac{T - T_c}{T_c} \right] .$$

The classical exponent $\frac{1}{2}$ of $r$ in (8) is compatible with earlier calculations of Moriya and Ueda[22] and Maniv.[10] For dimensions $1 < d \neq 3$, one must replace $r^{-1/2}$ by $r^{-(2-d/2)}$. The coefficient in large parentheses is connected with the fluctuation effect on $T_1^{-1}$, due to the strong anisotropy of the electronic system. From the work of Bourbonnais et al.,[23] it is also interesting to note that the 1D auxiliary susceptibility factor $Z_{1D}(T_x)$ in (8) coincides precisely with the 1D SDW fluctuation contributions to $T_1^{-1}$, namely that

$$Z_{1D}(T_x) = \sum_{|q| < T_x/V_F} \chi_{1D}''(q, \omega_N) / \omega_N .$$

On the other hand, the region $T_x > T \gg T_c$, $\chi'' \approx \chi_0'' Z_{1D}$, and we recover with (7a) the Korringa law $(T_1 T)^{-1} = \mathrm{const}$. Therefore, as a function of the temperature, $(T_1 T)^{-1}$ can be separated in the following three different contributions:

$$(T_1 T)_{1D}^{-1} = K C_{1D}(T/E_0)^{-\gamma_{1D}} \quad (E_0 > T > T_x) , \qquad (9a)$$

$$(T_1 T)_{\mathrm{Kor}}^{-1} = K Z_{1D}(T_x) \quad (T_x > T \gg T_c) , \qquad (9b)$$

$$(T_1 T)_{\mathrm{cr}}^{-1} = K Z_{1D}(T_x) \left[ \frac{d_a d_1^2}{\pi \xi_{0,a} \xi_{0,b} \xi_{0,c}} \right] r^{-1/2}$$

$$(r \ll 1) , \qquad (9c)$$

where $K = \pi \gamma_N^2 [\rho(E_F)]^2 \langle | \overline{A} |^2 \rangle$ and $C_{1D}$ is a 1D microscopic constant.[23] $\gamma_{1D}$ is the 1D auxiliary suscepti-

bility exponent $[Z_{1D}(T) = C_{1D}(T/E_0)^{-\gamma_{1D}}]$. A point of major importance here concerns the 3D critical form (9c) for $(T_1 T)^{-1}$, which has the well-known general scaling form predicted in the theory of critical phenomena for anisotropic systems.[24] Indeed, in the notation of Pfeuty et al.,[25] for example, the form (9c) can be written like

$$(T_1 T)_{\mathrm{cr}}^{-1} = A_\infty t_b^{-(v-\dot{v})/\phi} (T - T_c)^{-\dot{v}} , \qquad (9d)$$

with $v = \gamma_{1D}$ and $\dot{v} = \frac{1}{2}$ as the critical exponents of $(T_1 T)^{-1}$ in the 1D and 3D regimes, respectively. $\phi = 1 - \Theta$ is the crossover exponent,[15] $t_b$ acts as the symmetry-breaking parameter, and $A_\infty$ is a complicated nonuniversal constant which does not depend explicitly on $t_b$. It is worth mentioning that the above general form of $(T_1 T)^{-1}$ can also be derived from the dynamic scaling properties of $\int d^d q \chi''(q, \omega) / \omega$ in (1) near the critical point.[26]

## IV. DISCUSSION

We can now focus on the $^1\mathrm{H}\text{-}(\mathrm{TMTSF})_2\mathrm{PF}_6$ data given in Fig. 3. As mentioned before, in the strongly enhanced rgion, Fig. 4 clearly shows that the 3D-RPA $r^{-1/2}$ dominates the critical region. On the other hand, we note from Fig. 3 and (9c) that the data fail to overcome the methyl-group effects on the Korringa regime that should take place at $T \gtrsim 13$ K. The $(T_1 T)^{-1} = \mathrm{const}$ law in this region was apparently present in the higher-field data of Andrieux et al.,[8] but no detailed analysis of the methyl-group contribution was performed for these data (see also the end of this section).

In the RPA we can estimate from (8) the region for $T_1^{-1}$ where a clear departure from the linear regime (9b) is expected to be observed, namely when $(T_1)_{\mathrm{cr}}^{-1}/$

$(T_1^{-1})_{Kor} \sim 1$. This defines the "critical width" in the RPA:

$$\Delta t_{RPA} = \Delta t_{RPA}^0 \frac{t_a^4}{t_b^2 t_c^2} , \qquad (10)$$

where

$$\Delta t_{RPA}^0 = [2\pi^4 V_F^4/g_2^4(T_x)][\xi_{0,a}(T_c)/d_a]^{-6}$$

stands for the isotropic contribution to fluctuations, which is quite small: $\Delta t_{RPA} \sim 10^{-10}$, if one takes $g_2(T_x)/2\pi V_f \lesssim 0.5$ in a weak-coupling picture of the transition for $(TMTSF)_2PF_6$ at ambient pressure. Experimentally, the data of Fig. 3 give $\Delta t \approx 0.1$, and one needs from (10) an anisotropy factor of $t_a^2/t_b t_c \sim 10^4$, which is in reasonable agreement with accepted values as mentioned before.[20,21]

As $(T_1 T)^{-1}$ behaves like a critical quantity, we can estimate the range of validity of the present RPA treatment near $T_c$ [cf. (9c)] by looking at the Ginzburg critical width $\Delta t_G$, which gives, in units of $T_c$, the region around $T_c$ where the RPA treatment is inapplicable and where nonclassical exponents for $(T_1 T)^{-1}$ should prevail. From the Landau-Ginzburg approximation of the free-energy functional,[27,15] it is given by

$$\Delta t_G = \Delta t_G^0 \frac{t_a^4}{t_b^2 t_c^2} . \qquad (11)$$

$\Delta t_G^0$ refers to the isotropic Ginzburg critical width that has the same structure as an isotropic Bardeen-Cooper-Schrieffer (BCS) superconductor and is therefore quite small:[28] $\Delta t_G^0 \sim 10^{-14}$. The factor of enhancement on the right-hand side of (11) comes from the anisotropy of the electronic spectrum and, from before, it is of the order of $10^8$. Consequently, it is not sufficient to allow an observable departure from the $r^{-1/2}$ law and, therefore, the RPA form (9c) can be considered a good approximation essentially everywhere near $T_c$.[29]

It is interesting to note that the above treatment should only apply for itinerant quasi-1D antiferromagnets. In fact, for a ferromagnet, the $q$ dependence of $\chi''(q,\omega)$ is quite different, as is effectively the case in the RPA limit[22] where $\chi_0''(q,\omega) \propto \omega/q$ and $(T_1 T)^{-1} \propto r^{-1}$ for $d = 3$. Physically, this means that the particular $q$ dependence for relaxation time of electronic spin excitations that compose uniform or staggered critical fluctuations becomes highly relevant for the dynamical part of $\dot{v}$.[26] Therefore, the analysis of $T_1^{-1}$ data alone in the critical regime allows a clear differentiation between the antiferromagnetic and the ferromagnetic ground state.

We would like to conclude by commenting on the data of Figs. 3 and 4 with another possible mechanism that can give rise to an antiferromagnetic ground state and to similar critical effects on $T_1^{-1}$. The longitudinal nesting of the Fermi surface through the vector $\mathbf{Q}_0 = (2k_F,0,0)$, for example, has recently been proposed as a possible driving force for SDW transitions in $(TMTSF)_2X$ compounds.[30] In that case, the vector $\mathbf{Q}_0$ is 1D and the nesting takes place in the 1D region $(T > T_x)$. In the RPA, this mechanism also yields to a $r^{-1/2}$ critical profile for $T_1^{-1}$ $(\dot{v} = \frac{1}{2})$ but there is no Korringa law outside $\Delta t_{RPA}$ because of 1D

antiferromagnetic correlations $(T_c > T_x)$. Though the longitudinal nesting model has not yet received any microscopic justification for $(TMTSF)_2X$ compounds, it emerges, however, that a clear distinction between this mechanism and the one used in the present work will only be possible by a detailed analysis of the nonuniform $(q \neq 0)$ contribution of correlations to the relaxation in the paramagnetic phase $(T > T_c)$. However, in order to avoid the methyl-group contribution to the $^1H$ relaxation in this temperature domain, an NMR experiment on $^{77}Se$ has to be prescribed.

## ACKNOWLEDGMENTS

## APPENDIX: DERIVATION OF THE STAGGERED RPA SUSCEPTIBILITY AT $T < T_x$

In the RPA the auxiliary SDW susceptibility corresponding to the series of diagrams of Fig. 5 is given by

$$\bar{\chi}' \equiv \frac{\partial \chi'}{\partial \chi_0'} = \left[ 1 + \frac{g_2}{2} \chi_0' \right]^{-2} . \qquad (A1)$$

For $(g_2/2)\chi_0' \ll 1$, this gives rise to the perturbation series of $\bar{\chi}$:

$$\bar{\chi}'(x) \simeq 1 - g_2 \chi_0'(x) + \cdots . \qquad (A2)$$

If we are interested in the 1D regime of correlations, we have, in the standard notation,[19]

$$\chi_0'(x) = (\pi V_F)^{-1} \ln \left| \frac{x = \max(T, V_F q, \omega)}{E_F} \right|$$

for the real part of $\chi_0'$. Due to the logarithmic structure of $\bar{\chi}'$, Solyóm[19] has shown that for $T < E_F$, $\bar{\chi}'$ is a scaling quantity which satisfies the homgeneity relation:

$$\bar{\chi}'(x/E_F) = Z_{1D}(E_0/E_F)[1 - g_2(E_0)\chi_0'(x/E_0) + \cdots ,$$
$$\qquad (A3)$$
$$\bar{\chi}'(x/E_F) = Z_{1D}(E_0/E_F)\bar{\chi}'(x/E_0) ,$$

where $x < E_0 < E_F$. $Z_{1D}(E_0/E_F)$ and $g_2(E_0)$ are, respectively, the real part of the 1D auxiliary $2k_F$ SDW susceptibility and the effective forward scattering coupling evaluated at $x = E_0$. Both can be evaluated using the renormalization-group method.[17,19] For the model proposed in Sec. III, the RPA expression for $\bar{\chi}$ near $\mathbf{Q}_0 = (2k_F, \pi/d_\perp, \pi/d_\perp)$ at $T < T_x$ can also be calculated via the diagrams of Fig. 5, except for the inclusion of the 1D $2k_F$ corrections for the energy range $T_x < E_0 < E_F$. This can be done by setting $E_0 = T_x$ in (A3) with the result

$$\bar{\mathcal{X}}'(q,\omega) = \frac{Z_{1D}(T_x)}{\{1+[g_2(T_x)/2]\mathcal{X}_0'(q,\omega)\}^2} \ . \tag{A4}$$

From the definition (A1) of $\bar{\mathcal{X}}$, we can write

$$\mathcal{X}'(q,\omega) = -\int_{\mathcal{X}_0'} \bar{\mathcal{X}}' d\mathcal{X}_0' = -\frac{[2/g_2(T_x)]Z_{1D}(T_x)}{1+[g_2(T_x)/2]\mathcal{X}_0'(q,\omega)} + C \ . \tag{A5}$$

$C$ is an integration constant that can be fixed by the 1D condition $\mathcal{X}' = \mathcal{X}'_{1D}$ when $T = T_x$. This gives $C = \mathcal{X}'_{1D}$

$+2Z_{1D}/g_2$ and we get, for the real part of $\mathcal{X}$,

$$\mathcal{X}'(q,\omega) = \frac{\mathcal{X}_0'(q,\omega) + \mathcal{X}'_{1D}(T_x)}{1+[g_2(T_x)/2]\mathcal{X}_0'(q,\omega)} \ . \tag{A6}$$

In the limit $\omega \to 0$, we can write, for the imaginary part,

$$\mathcal{X}''(q,\omega) = \mathcal{X}_0''(q,\omega)\bar{\mathcal{X}}'(q,\omega) \quad (\omega \to 0) \ , \tag{A7}$$

and from (A5), this finally leads to the expression

$$\mathcal{X}''(q,\omega) = \frac{Z_{1D}(T_x)\mathcal{X}_0''(q,\omega)}{\{1+[g_2(T_x)/2]\mathcal{X}_0'(q,\omega)\}^2} \ . \tag{A8}$$

[1]W. M. Walsh, F. Wuld, G. A. Thomas, D. Nalewajek, J. J. Hauser, P. A. Lee, and T. Poehler, Phys. Rev. Lett. **45**, 829 (1980).

[2]P. M. Chaikin, G. Grüner, E. M. Engler, and R. L. Greene, Phys. Rev. Lett. **45**, 1874 (1980).

[3]J. C. Scott, H. J. Pederson, and K. Bechgaard, Phys. Rev. Lett. **45**, 2125 (1980).

[4]H. J. Pedersen, J. C. Scott, and K. Bechgaard, Solid State Commun. **35**, 207 (1980).

[5]K. Mortensen, Y. Tomkiewicz, and K. Bechgaard, Phys. Rev. B **25**, 3319 (1982).

[6]K. Mortensen, Y. Tomkiewicz, T. D. Schultz, and E. M. Engler, Phys. Rev. Lett. **46**, 1234 (1981).

[7]J. B. Torrance, H. J. Pedersen, and K. Bechgaard, Mol. Cryst. Liq. Cryst. **86**, 255 (1982).

[8]A. Andrieux, D. Jérome, and K. Bechgaard, J. Phys. (Paris) Lett. **42**, L87 (1981).

[9]J. C. Scott, H. J. Pedersen, and K. Bechgaard, Phys. Rev. B **24**, 475 (1981); P. C. Stein, A. Moradpour, and D. Jérome, J. Phys. (Paris) Lett. **46**, L241 (1985).

[10]T. Maniv, Solid State Commun. **43**, 47 (1982); H. Morawitz and J. C. Scott, Mol. Cryst. Liq. Cryst. **85**, 305 (1982).

[11]S. Clough, J. Phys. C **15**, 2495 (1982).

[12]S. Toffano, Troisième Cycle thesis, Université de Paris—Sud, Orsay, 1985 (unpublished).

[13]C. Coulon, P. Delhaes, S. Flandrois, R. Langier, E. Bonjour, and J. M. Fabre, J. Phys. (Paris) **43**, 1059 (1982).

[14]V. J. Emery, R. Bruisma, and S. Barišić, Phys. Rev. Lett. **48**, 1039 (1982).

[15]C. Bourbonnais, Mol. Crys. Liq. Cryst. **119**, 11 (1985); Ph.D. thesis, Université de Sherbrooke, 1985 (unpublished).

[16]V. J. Emery, J. Phys. (Paris) Colloq. **44**, C3-977 (1983).

[17]V. N. Prigodin and Y. A. Firsov, Zh. Eksp. Teor. Fiz. **76**, 1602 (1979) [Sov. Phys.—JETP **49**, 813 (1979)].

[18]T. Moriya, J. Phys. Soc. Jpn. **18**, 516 (1963).

[19]J. Solyóm, J. Low Temp. Phys. **12**, 547 (1973).

[20]P. M. Grant, J. Phys. (Paris) Colloq. **44**, C3-847 (1983).

[21]D. Jérome and H. J. Schulz, Adv. Phys. **31**, 299 (1982).

[22]T. Moriya and K. Ueda, Solid State Commun. **15**, 169 (1974).

[23]C. Bourbonnais, F. Creuzet, D. Jérome, K. Bechgaard, and A. Moradpour, J. Phys. (Paris) Lett. **45**, L755 (1984).

[24]E. Riedel and F. Wegner, Z. Phys. **255**, 195 (1969).

[25]P. Pfeuty, D. Jasnow, and M. E. Fisher, Phys. Rev. B **10**, 2088 (1974).

[26]C. Bourbonnais (unpublished).

[27]S. Barisic and S. Marcelja, Solid State Commun. **7**, 1395 (1969).

[28]G. L. Ginzburg, Fiz. Tverd. Tela (Leningrad) [Sov. Phys.—Solid State **2**, 1824 (1961)].

[29]It must be emphasized that for the expressions (10) and (11) of $\Delta t_{RPA}$ and $\Delta t_G$ we have not included the 1D self-energy corrections due to correlations which are at the origin of the reduction of the crossover temperature $T_x^0$ by the factor $d(T_x) = (T_x/E_F)^\Theta < 1$, where $T_x$ is the true crossover temperature. Taking into account this reduction is equivalent to making the substitution $t_{b,c} \to d(T_x)t_{b,c}$ in all calculations leading to $\Delta t_{RPA,G} = d^{-4}(T_x)\Delta t_{RPA,G}^0(t_a^4/t_b^2 t_c^2)$. The value of $\Theta$ is expected to be small, however ($\Theta < 1$), so that the additional increase of $\Delta t_{RPA}$ and $\Delta t_G$ should not be very large.

[30]L. P. Gorkov and A. Lebed, Mol. Cryst. Liq. Cryst. **119**, 73 (1985).